ACS Photonics

Article

Cite This: ACS Photonics XXXX, XXX, XXX−XXX

pubs.acs.org/journal/apchd5

Hybrid Full-Color Inorganic Light-Emitting Diodes Integrated on a Single Wafer Using Selective Area Growth and Adhesive Bonding

Chang-Mo Kang,[†] Jun-Yeob Lee,[†] Duk-Jo Kong,[‡,§] Jae-Phil Shim,[∥] Sanghyeon Kim,[∥] Seung-Hyun Mun,[†] Soo-Young Choi,[†] Mun-Do Park,[†] James Kim,[⊥] and Dong-Seon Lee*[,†]

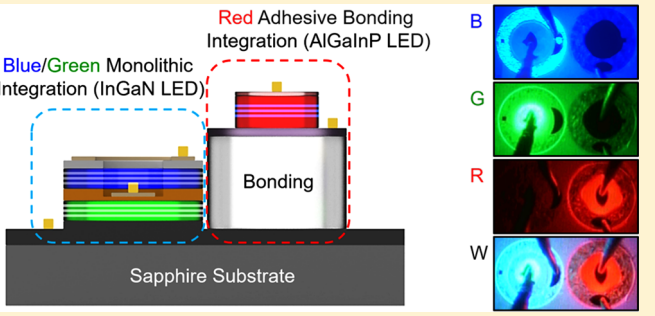
[†]School of Electrical Engineering and Computer Science, [‡]Advanced Photonics Research Institute, and [§]Future Research Center, Gwangju Institute of Science and Technology (GIST), 123 Cheomdangwagi-ro, Buk-gu, Gwangju 61005, Korea

[∥]Korea Institute of Science and Technology (KIST), 5, Hwarang-ro 14-gil, Seongbuk-gu, Seoul 02792, Korea

[⊥]Sundiode, Inc., 1030 El Camino Real, Sunnyvale, California 94087, United States

Supporting Information

ABSTRACT: In recent years, research into implementing microdisplays for use in virtual reality and augmented reality has been actively conducted worldwide. Specifically, inorganic light-emitting diodes (LED) have many advantages in microdisplays, so much effort has been made to implement them in various ways. However, it is still challenging to realize a display with high resolution using only inorganic LEDs without color conversion layers because a typical LED chip is designed to emit only one color on a single wafer. In this study, we integrated high-efficiency red, green, and blue (RGB) LED material systems on the same sapphire substrate. Since the blue and green LED structures comprised the same GaN semiconductor, a metalorganic chemical vapor deposition method was used to integrate them. Meanwhile, the red LEDs made from another semiconductor were incorporated into the blue/green LEDs using a wafer-bonding technique. The fabricated hybrid RGB LEDs were able to cover a wide color space. In addition, the RGB LED material systems consisting of a high-quality single crystal were stably combined on the sapphire substrate without any structural defects. We show the possibility of their use in displays by integrating the RGB LEDs on one chip and suggest that their utilization could range from large-area LED displays to ultrahigh-resolution small displays.



KEYWORDS: *micro LEDs, micro displays, selective area growth (SAG), wafer bonding, RGB full color, monolithic integration*

Downloaded via GWANGJU INST SCIENCE & TECHNOLOGY on October 10, 2018 at 02:15:41 (UTC).
See https://pubs.acs.org/sharingguidelines for options on how to legitimately share published articles.

Inorganic light-emitting diodes (LEDs) are made of single-crystal compound semiconductors, so they have higher luminous efficiency and stronger durability than other light sources such as incandescent lamps, fluorescent lamps, and organic LEDs.[1] Due to these advantages, inorganic LEDs have been widely used not only in lighting but also in display applications such as digital signage and the backlight of liquid crystal displays.[2,3] However, in the display industry, there is a growing demand for self-emitting displays with a very wide color gamut and high resolution.

Recently, as the interest in microdisplays for use in virtual reality and augmented reality has increased, much effort has been made to adopt highly efficient inorganic LEDs as a light source for these applications.[4−6] However, it is difficult to realize a display with high resolution using conventional inorganic LED manufacturing technology alone. First, there is a limit on reducing the size of the LED chip itself. When cutting a thick LED wafer using a laser or a dicing saw, a kerf loss of a few tens of μm or more occurs around the chip; thus, the chip size cannot be smaller than the kerf loss size.[7,8] Second, it is difficult to realize highly efficient red, green, and blue (RGB) emissions on a single wafer, because the material system of the high-efficiency red LED structure is different from those of the high-efficiency blue and green LED structures. Theoretically, the InGaN material system can cover the entire visible spectrum from infrared (0.69 eV) to ultraviolet (3.4 eV) by varying the composition of In in an InGaN alloy.[9] However, it is difficult to form high-quality InGaN films with excessive compositions of In experimentally due to its re-evaporation from the growth surface.[10] In addition, the internal and external quantum efficiencies of InGaN-based LEDs decrease abruptly toward the red spectral region.[11] In short, it is challenging to realize high-efficiency red emission (~630 nm) from InGaN/GaN LEDs. For these reasons, an InGaN LED structure has been used for high-efficiency green and blue emission and a high-efficiency AlGaInP LED structure has been used for red emission.[12,13] In other words, each RGB LED chip fabricated from three

Received: June 29, 2018
Published: September 25, 2018

© XXXX American Chemical Society

DOI: 10.1021/acsphotonics.8b00876
ACS Photonics XXXX, XXX, XXX−XXX

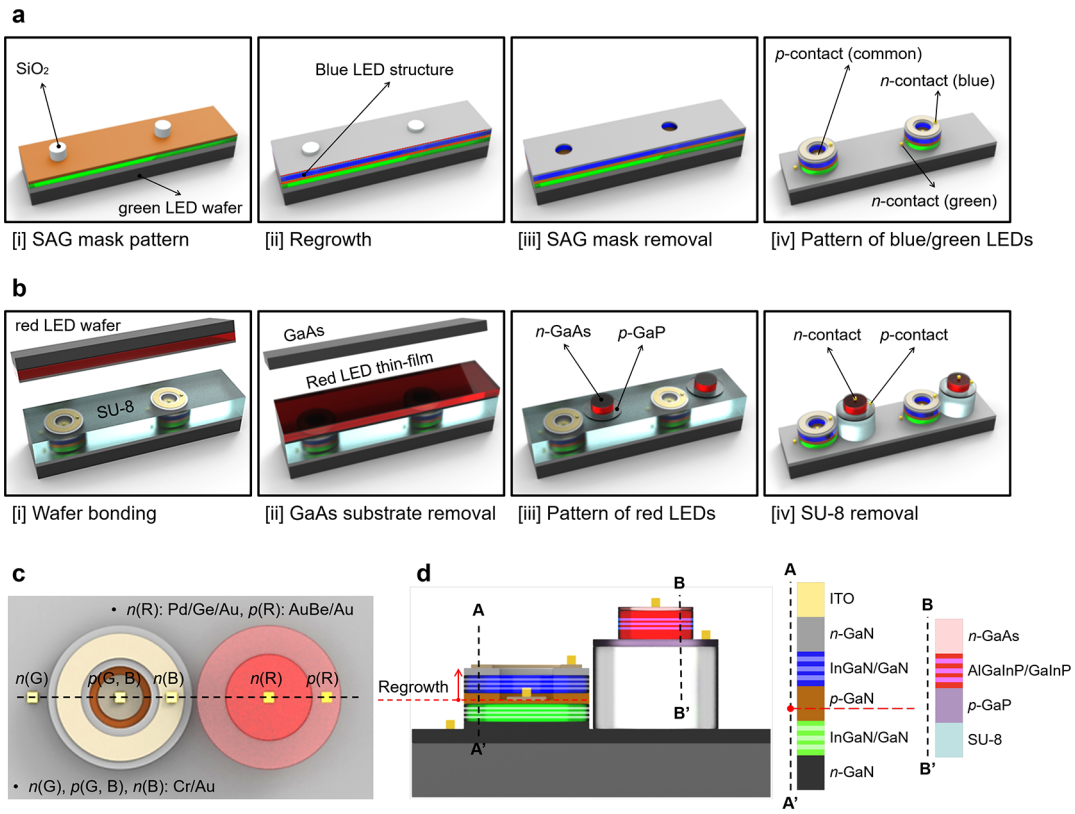


Figure 1. Schematic of the fabrication process of the hybrid RGB LEDs: (a) the fabrication process of the blue/green dual-color LEDs using selective area growth (SAG), (b) the process for the formation of the red pixels using adhesive bonding, and (c) top and (d) cross-sectional views of the final device.

different LED wafers was required to form a pixel, resulting in a limitation in resolution.

Several epitaxial structures and fabrication methods have been suggested to emit various colors on a single wafer. Some research groups have introduced InGaN/GaN structures with multifacets, such as nanorods, pyramids, and donuts, and demonstrated various color emissions by varying the current injection density into GaN multifacets.[14−17] Other groups have implemented polychromatic wavelengths by vertically or laterally growing two or more active regions with different emission wavelengths.[18,19] However, it is difficult to independently control both each RGB color and its brightness because all LEDs using these methods have only two electrode terminals in common. These methods could be suitable for implementing white LEDs for illumination rather than the application of a display direct light source.[20]

Much research has been carried out recently to achieve high-resolution microdisplays by arranging RGB LED thin films accurately and effectively, resulting in a pixel size of under a few tens of micrometers.[21−24] Currently, the most widely attempted methods for creating micro-LEDs are picking and placing a number of LED thin films without a substrate via laser lift-off (LLO) or chemical lift-off. The major technical issue with this approach is acquiring all of the RGB thin-film LED pixels and placing them on the display panel without any missing pixels. Therefore, many research groups and companies are studying this methodology and attempting to solve the problem of transfer yield. Nevertheless, the thin-film LED pixel transfer method still has a limited resolution because it depends on the pick-and-place machine accuracy rather than the photolithography resolution. In short, this thin-film LED pixel transfer method may be suitable for 100−400 pixel-per-inch (PPI) level display applications, such as smart watches, TVs, and mobile phones. However, higher-resolution displays above 1000−2000 PPI, such as head-mounted displays, smart glasses, and pico projectors, remain a challenge.

Other research groups have attempted monolithic methods that form a lot of pixels using only a photolithography process on a single wafer to achieve a higher resolution than the pick-and-place method.[25] For example, CEA-LETI implemented monochromatic micro-LEDs with a resolution of approximately 2500 PPI using a monolithic method.[26] Here, the biggest challenge with the monolithic approach is realizing RGB full color, and many research groups have tried this in a variety of ways such as with wavelength conversion layers and nanowires.[27−29] However, to achieve ultrahigh-resolution displays with both a very wide color space and high efficiency, it is advantageous to form RGB self-emitting light sources rather than wavelength conversion layers on a single wafer.

In this study, we demonstrated the integration of red (AlGaInP), green (InGaN), and blue (InGaN) LEDs composed of high-efficiency inorganic material systems onto a single wafer and showed their applicability for displays. To realize this, we first attempted to integrate both the green and the blue LEDs composed of the same material system (InGaN) monolithically on a sapphire substrate through a selective area growth (SAG) method (Figure 1a). Next, for the realization of the red LEDs, a highly efficient AlGaInP system was combined with an InGaN system via an adhesive bonding technique (Figure 1b). A detailed description of the fabrication process is presented in the Methods section. Unlike conventional methods that require repetitively picking-and-placing

DOI: 10.1021/acsphotonics.8b00876
ACS Photonics XXXX, XXX, XXX−XXX

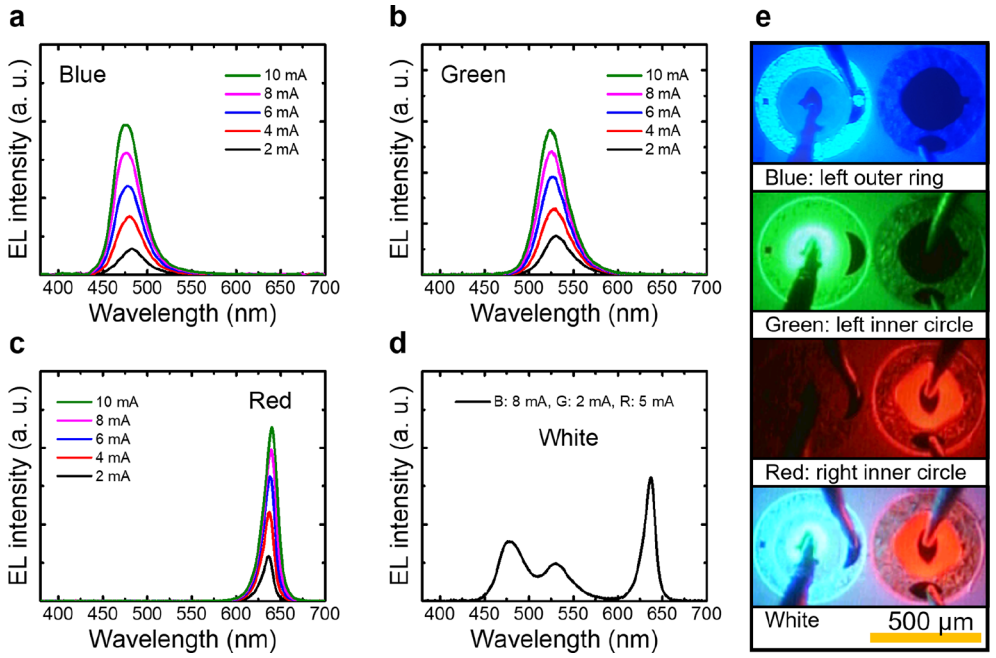


Figure 2. Electroluminescence (EL) spectra of the (a) blue, (b) green, and (c) red LEDs measured by varying the injection current (2, 4, 6, 8, and 10 mA), (d) an EL spectrum of a hybrid RGB LED in the white mode (blue, 8 mA; green, 2 mA; red, 5 mA), and (e) microscopic images of the hybrid RGB LEDs in (top to bottom) blue, green, red, and white color modes.

Table 1. Peak Wavelengths and fwhms of the EL Spectra for the Hybrid RGB LEDs Measured by Varying the Injection Current (2, 4, 6, 8, and 10 mA)

	blue LED					green LED					red LED				
injection current (mA)	2	4	6	8	10	2	4	6	8	10	2	4	6	8	10
peak wavelength (nm)	482	479	477	476	476	530	529	527	525	524	636	637	638	639	640
fwhm (nm)	33	35	35	35	35	35	37	37	37	37	14	15	16	17	18

each RGB pixel, we only used a standard semiconductor process on a single wafer, entailing a potential to improve the resolution and pixel yield. In addition, it is meaningful in that RGB full-color LEDs were realized without the high-cost LLO or a color conversion material. We analyzed the operation and color of the fabricated hybrid RGB LEDs using electroluminescence (EL) measurements, and their overall structure and unique characteristics were intensively studied using scanning electron microscopy (SEM), transmission electron microscopy (TEM), microphotoluminescence (μ-PL), and atomic force microscopy (AFM).

RESULTS AND DISCUSSION

EL Spectra of the Hybrid RGB LEDs. In general, the color and brightness of a pixel in a display are determined by the grayscale of each RGB light source. In this experiment, we controlled the grayscale of the hybrid RGB LEDs by varying the injection current, as shown in the EL spectra of each RGB LED (Figure 2a–c). As the injection current applied to each RGB LED increased from 2 to 10 mA in 2 mA increments, the EL intensity of each RGB LED was increased by dividing it into five gray levels (one for each increment). Here, the EL peak wavelengths and full-widths at half-maximum (fwhms) of the blue, green, and red LEDs were 479 and 35 nm, 529 and 37 nm, and 637 and 15 nm, respectively (@ 4 mA). However, the spectra exhibited peak wavelengths that were slightly shifted as the injection current increased (Table 1). The peak wavelengths of the InGaN/GaN-based blue and green LEDs were blue-shifted due to the band-filling effect, while the peak wavelength of the AlGaInP-based red LEDs was red-shifted due to the Joule-heating effect caused by the lower thermal conductivity of the SU-8 (0.3 W/m °C) than GaAs (55 W/m °C).[30−32] In addition to the monochromatic blue, green, and red emission, we were able to attain the white color by manually tuning the injection currents applied to each RGB LED, as shown in Figure 2d. The spectrum of the white color had triple peak wavelengths at 476, 530, and 637 nm. As a result, each RGB LED was independently operated in its respective emission region, which is shown in the microscope images of the device in Figure 2e.

Additive Color Mixing of Hybrid RGB LEDs. In a display using inorganic LEDs as a self-radiative light source, the color of a pixel is produced by the additive color mixing of the three light sources (the RGB LEDs). To express the desired color accurately, it is important to control the optical power of each light source. Equations 1–4 represent the relationship between the three light sources' optical powers and the chromaticity coordinates of the produced color:

$$L_1 = \bar{x}(\lambda_1)P_1 + \bar{y}(\lambda_1)P_1 + \bar{z}(\lambda_1)P_1 \quad (1)$$

$$L_2 = \bar{x}(\lambda_2)P_2 + \bar{y}(\lambda_2)P_2 + \bar{z}(\lambda_2)P_2 \quad (2)$$

$$L_2 = \bar{x}(\lambda_3)P_3 + \bar{y}(\lambda_3)P_3 + \bar{z}(\lambda_3)P_3 \quad (3)$$

$$x = \frac{x_1L_1 + x_2L_2 + x_3L_3}{L_1 + L_2 + L_3}, \quad y = \frac{y_1L_1 + y_2L_2 + y_3L_3}{L_1 + L_2 + L_3} \quad (4)$$

DOI: 10.1021/acsphotonics.8b00876
ACS Photonics XXXX, XXX, XXX−XXX

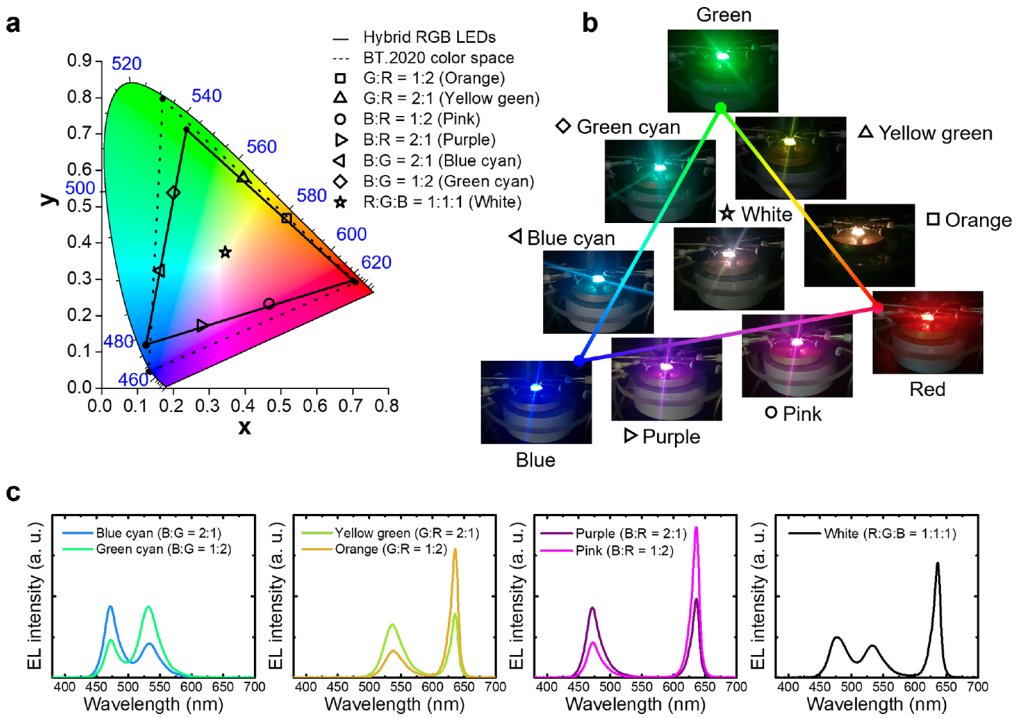


Figure 3. Color performance of the hybrid RGB LEDs: (a) chromaticity coordinates, (b) photographs for 10 color modes, and (c) EL spectra for two- and three-color mixing.

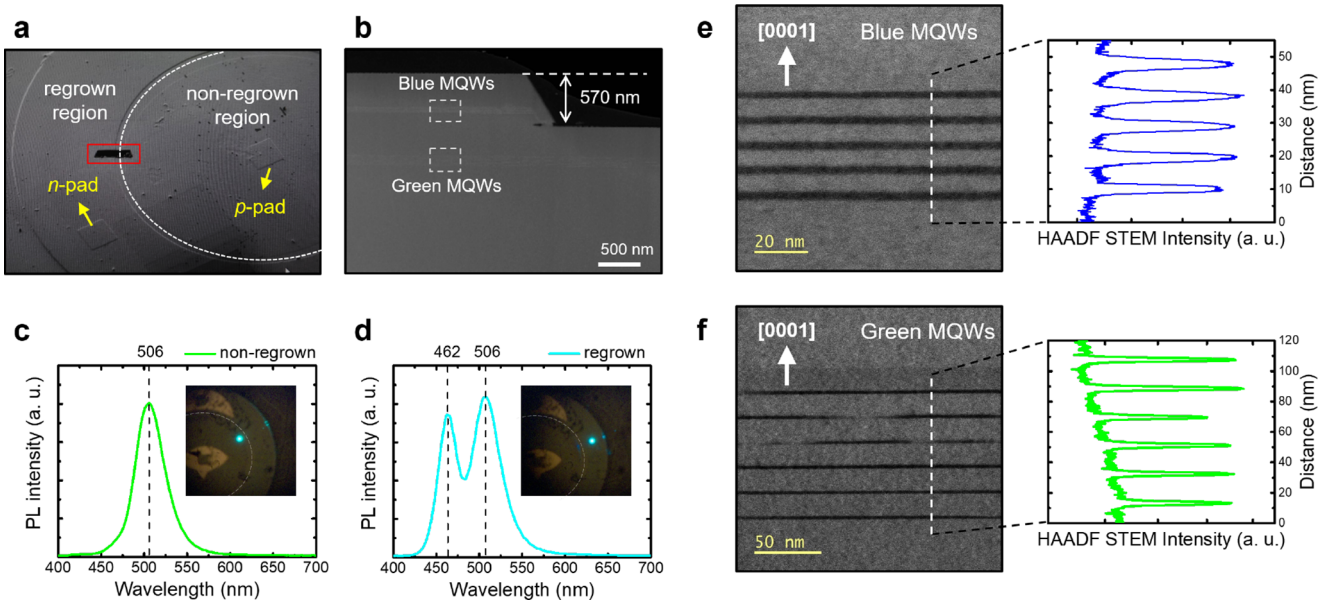


Figure 4. (a) Tilted-view scanning electron microscopy (SEM) image of the dual LEDs, and (b) a low magnified cross-sectional scanning transmission electron microscopy (STEM) image of the regrown boundary region, microphotoluminescence (PL) plots of the (c) nonregrown and (d) regrown regions, and high-magnification STEM images of the (e) blue and (f) green MQWs.

where $[\bar{x}(\lambda), \bar{y}(\lambda), \bar{z}(\lambda)]$, $[P_1, P_2, P_3]$, and $[(x_1, y_1), (x_2, y_2), (x_3, y_3)]$ are the color matching functions, optical powers, and chromaticity coordinates of the three light sources, respectively.

This optical power can be controlled by varying the injection current or the duty ratio of the pulse-width modulation according to the driving circuit.[33,34] In this experiment, we controlled the optical power by tuning the injection current, and the ten-color modes were produced as follows: [(blue/green/red)] = [(3:0:0), (2:1:0), (1:2:0), (0:3:0), (0:2:1), (0:1:2), (0:0:3), (1:0:2), (2:0:1), (1:1:1)] (Supporting Information 1, Table S1).

We first measured the CIE chromaticity coordinates of individual RGB LEDs to check the color range that the hybrid RGB LEDs were able to express. As shown by the CIE coordinates in Figure 3a, the fabricated LEDs were able to cover the RGB full-color range. Specifically, the color space of the hybrid RGB LEDs (solid line) covered approximately 80% of the BT.2020 color space (dashes) used as the color evaluation item in an ultrahigh definition display, thus,

DOI: 10.1021/acsphotonics.8b00876
ACS Photonics XXXX, XXX, XXX−XXX

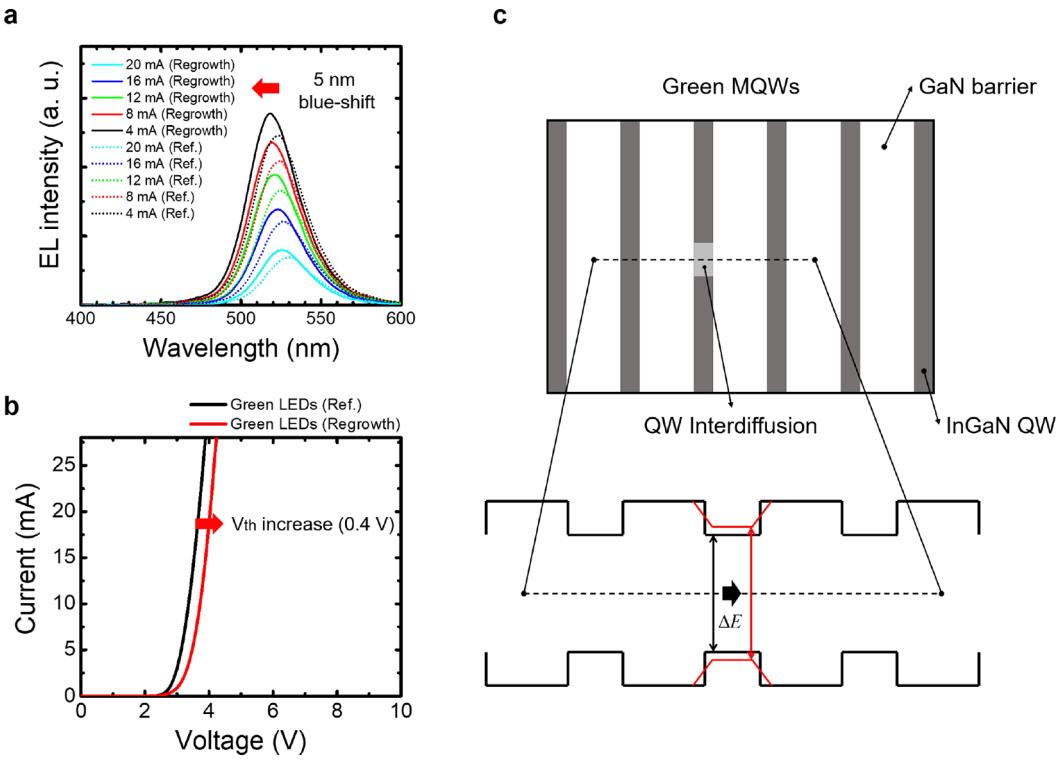


Figure 5. (a) Electroluminescence (EL) spectra and (b) current−voltage (I−V) characteristics of the green LEDs with/without the regrowth process. (c) Schematic diagram illustrating the mechanism for the change in electrical and optical properties caused by regrowth.

demonstrating a fairly wide color space.[35] Although the color space of the hybrid RGB LEDs is narrower in the blue and green regions compared to the BT.2020 color space, we expect that the color coordinates near these regions can be expanded further by tuning the growth parameters of InGan/GaN and shifting the blue and green light's emission wavelengths toward 467 and 532 nm, respectively.

Not only the CIE coordinates of the individual RGB LEDs, but also those of two- and three-color mixing were measured to verify that color control was as intended. The chromaticity coordinates of the two-color mixing were plotted on a straight line connecting those of the two light sources to approximately three equal parts. In short, each chromaticity coordinate of the mixed light became the internal division point weighted by the optical power ratios of the two light sources. Moreover, the chromaticity coordinates in the white mode were located in the center of gravity of the color triangle.

Figure 3b presents a series of photographic images corresponding to the CIE chromaticity coordinates in Figure 3a. The hybrid RGB LEDs emitted various light colors ranging from blue (~475 nm) to red (~635 nm) and even to colors that could not be realized with a monochromatic wavelength (pink and white). In addition, the colors of the mixed light were consistent with those of the chromaticity coordinates in Figure 3a. The EL spectra for the two- and three-color mixing had a spectrum shape that superimposed the individual spectrum of each light source (Figure 3c). In conclusion, through measurements of the chromaticity coordinates and the EL spectra, we demonstrated that the hybrid RGB LEDs covered a very wide range of full colors and could be controlled as intended.

Analysis of the Regrown Epistructure of the Monolithic Dual LEDs. Figure 4a shows a tilted-view SEM image of the dual LEDs, in which the white dotted line represents the boundaries between the regrown and non-regrown epilayers. For an in-depth analysis, a TEM specimen was prepared, as indicated by the red lines in Figure 4a. In the high-angle annular dark-field scanning transmission electron microscopy (HAADF-STEM) images (Figure 4b), it can be seen that the regrown epilayer consisted of two active regions laminating the blue and green MQWs. The thickness of the regrown epilayer (p-GaN/MQWs/n-GaN) was approximately 570 nm (140/50/380 nm), which was much thinner than that of a typical LED epilayer. This monolithic blue/green integration is significantly meaningful in that the use of the sapphire substrate and the total growth time were reduced, thus resulting in cost savings when compared with the conventional method requiring three LED wafers.

To understand the multijunction structure of the monolithic dual LEDs more fully, μ-PL measurements were conducted, the results of which were compared with the EL results (Figure 2). The nonregrown region consisted of only green MQWs, so only a single peak wavelength of 506 nm was observed in the inner circle (Figure 4c). In contrast, two peaks at wavelengths of 460 and 506 nm were observed in the regrown region (ring-shaped) because it consisted of both blue and green MQWs (Figure 4d). Although the dual peak wavelength from the PL excitation was observed in the regrown region (ring-shaped), the green EL emission in this region could not be intentionally produced, as shown in Figure 2e. This is because the holes in the p-GaN material were only injected into the green MQWs in the nonregrown region (inner circle) with a current spreading layer. In other words, the green MQWs in the regrown region (ring-shaped) were not used as a radiative recombination layer.

Meanwhile, in the regrown region (ring-shaped) laminating the two different active regions, an unintended optical absorption phenomenon could occur due to the interactions

DOI: 10.1021/acsphotonics.8b00876
ACS Photonics XXXX, XXX, XXX−XXX

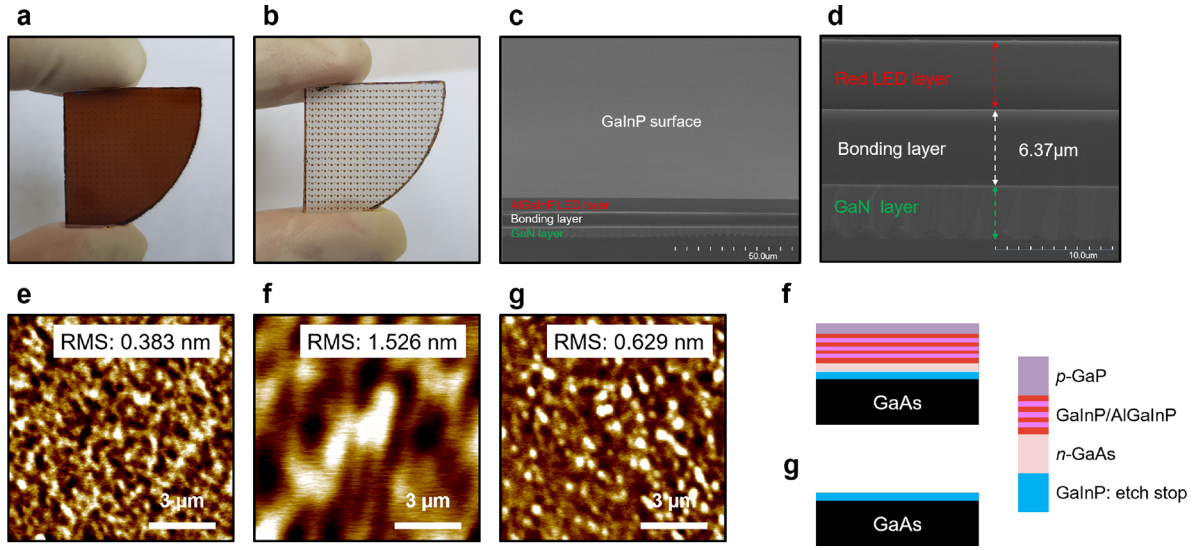


Figure 6. Bonding reliability of the hybrid RGB LEDs: photographs of (a) the AlGaInP-based red LED thin film transferred completely onto the blue/green dual LED chip and (b) the sample where the red pixel was formed through the photolithography process, (c) tilted-view and (d) cross-sectional scanning electron microscopy (SEM) images of the transferred red LED thin film, and atomic force microscopy (AFM) images of (e) the transferred red LED thin film, (f) the red LED wafer, and (g) the red LED wafer etched from the *p*-GaP surface down to the etching stop layer.

between the energy bandgaps and emission wavelengths of the two different active layer regions. Specifically, as the intensity of the blue EL emission generated in the blue MQWs (ring-shaped) increased, the unintended PL excitation in the underlying green MQWs (ring-shaped) could be generated by the blue EL emission because the green MQWs (~2.34 eV) absorbed the blue light (~2.65 eV). However, as can be seen in Figure S1a, only a single wavelength of 475 nm was observed despite applying a high current to the blue LED. In short, the influence of the green PL excitation caused by the blue EL emission was negligible, so no unintended color modulation was observed (Supporting Information 2, Figure S1).

Figure 4e and f shows high magnification HAADF-STEM images of the blue and green MQWs, respectively. The upper active region emitting the blue light is uniformly comprised of five-period MQWs. Meanwhile, in the case of the underlying green active region consisting of six-period MQWs, a few points of QWs had lower HAADF-STEM intensity than the others. This lack of uniformity of the green MQWs appears to have occurred during the regrowth process. To understand how this affected the green LEDs, we prepared green LEDs fabricated without the regrowth process as a reference. For a fair comparison, both the regrown and reference samples were extracted from the same green LED wafer and the same fabrication process was carried out simultaneously, except for the regrowth step. The EL spectra and the current−voltage (*I*−*V*) characteristics of the green LEDs of the two samples are displayed in Figure 5a and b, respectively. It can be seen that the EL spectrum of the regrown sample was blue-shifted by 5 nm compared to the reference sample at the same current injection. In the electrical characteristics of the regrown samples, there was little change in the series resistance and only the turn-on voltage increased by 0.4 V. These slight changes in the optical and electrical properties of the green LED are probably due to the unintended QW interdiffusion[36] that occurs during the regrowth (Figure 4f). Due to the effect of the regrowth temperature (~960 °C), which was relatively higher than the active region growth temperature (~750 °C) during regrowth, the indium in the MQWs slightly interdiffused into the adjacent region, thereby causing a reduction in their indium content. This resulted in the energy band gap in some of the MQWs becoming larger than before the regrowth (Figure 5c). This change in bandgap energy directly affected the emission wavelength ($\lambda = hc/E_g$) and turn-on voltage ($V_{th} = E_g/e$), so the phenomenon causing the blue-shifted spectrum and the turn-on voltage increase was well interpreted by the QW interdiffusion mechanism.

Although the changes in the optical and electrical characteristics of the green LEDs after regrowth are not severe, optimization studies to minimize unintended QW interdiffusion are needed to acquire high-quality two-color emission wavelengths. However, the regrowth process should be designed in consideration of not only the unintended QW interdiffusion of the underlying LED structure, but also the regrown epitaxial quality, since the crystallinity of the GaN material may be adversely affected when the regrowth temperature is set too low.[37] We used high-resolution transmission electron microscopy (HRTEM) to check the crystallinity of the two active regions (Supporting Information 3, Figure S2). The interplanar spacings of the c-GaN barriers in both the blue and green active regions measured from the HRTEM images were approximately 5.2 Å, which was almost consistent with the lattice constant of GaN (c = 5.186 Å). In addition, the clear diffraction patterns of the fast Fourier transform (FFT) were regularly arranged, confirming that the blue and green active regions had a high-quality monocrystalline.

Analysis of the Bonding of the AlGaInP-Based Red LEDs. To implement the red pixels using our adhesive bonding strategy, the entire red LED thin film was transferred onto a dual LED chip through GaAs substrate removal and then pattered via a standard semiconductor fabrication process. Although we used a commercial red LED wafer designed for substrate removal in this experiment, replacing the substrate removal process with an epitaxial lift-off process by inserting a sacrificial layer into the red LED structure will further improve the process throughput and provide donor wafer reusability, thus, resulting in a cost reduction.[38,39]

DOI: 10.1021/acsphotonics.8b00876
ACS Photonics XXXX, XXX, XXX−XXX

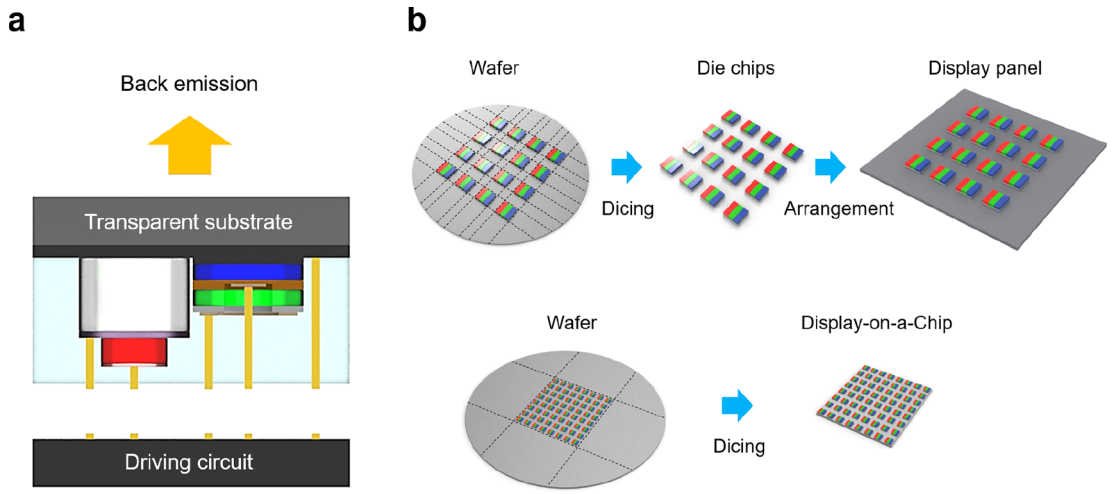


Figure 7. Concept Schematic of (a) the Flip-Chip Structure and (b) Various Display Applications Using the Hybrid RGB LEDs.

The important point of our bonding technique is that the thin-film LED is transferred only once without an intermediate substrate, which could be advantageous in terms of transfer yield. The bonding transfer yield of the AlGaInP red thin film can be best visualized in the photographic image in Figure 6a. We succeeded in transferring the entire red LED film at a yield of almost 100% on the dual LED chip with a quarter-sized 2-in. wafer. Furthermore, in the sample where the red pixels were formed through the photolithography process, there were no missing pixels among approximately 350, as shown in Figure 6b, because the red pixel yield was directly related to the transfer yield of the entire thin film.

To check whether the transferred red LED thin film was stably bonded, the bonding interface of the sample was observed via the SEM images in Figure 6c,1d. The bonding material integrated the AlGaInP/InGaP and InGaN/GaN systems without any air gaps or cracks, and the transferred red LED epilayer additionally showed no cracks or damage. To further study the transferred red LED thin film, its surface was measured using AFM, as shown in Figure 6e–g. The root-mean-square (RMS) of the surface roughness of the transferred LED was 0.383 nm, which was lower than the red LED wafer's surface RMS (1.526 nm). However, the surface of the red LED wafer was *p*-GaP, which differed from the surface (etching stop layer: GaInP) of the transferred red LED thin film. For a similarity comparison, a reference sample was prepared by wet-etching the red LED wafer down to the etching stop layer from the *p*-GaP surface. The surface RMS of the reference sample was 0.629 nm, confirming that the surface of the transferred red LED was fairly uniform. It is worth noting that the AlGaInP-based and InGaN-based LEDs were stably integrated by the adhesive bonding without any transfer-yield degradation of the red pixels.

Relevance of the Hybrid RGB LEDs for Display Applications. For the fabricated hybrid RGB LEDs to be applied in an actual display, they should be connected to the latter's drive circuit, such as CMOS or TFT. However, since the hybrid RGB LEDs are composed of a stacking structure, their electrodes are located at different heights. For this reason, the position of their metal electrodes should be set to the same height; thus, planarization and via-hole technologies may be required. In this study, the hybrid RGB LEDs were probed in the forward direction for easy and precise optical measurements. However, a flip-chip structure that emits light toward the reverse side of the chip is more suitable for display applications.[40] In this case, the hybrid RGB LEDs emit light behind the chip through a transparent substrate, such as double-side-polished sapphire (Figure 7a). Using this flip-chip structure, the hybrid RGB LEDs could be used in various applications ranging from low-resolution displays in which the diced RGB LED chips are individually arranged to high-resolution displays in which the RGB chip itself becomes a display panel (Figure 7b).

METHODS

Integration of the Blue and Green InGaN/GaN LEDs. InGaN/GaN-based blue and green LED structures were monolithically integrated on a sapphire substrate via the SAG technique (Figure 1a). First, a 500 nm thick SiO_2 film was deposited on the green LED wafer using plasma-enhanced chemical vapor deposition and 300 μm diameter circle SAG masks were formed using a standard photolithography process (Figure 1a-i). When forming the SAG mask, a buffered oxide etchant (BOE) wet-etching process was used instead of dry etching to minimize *p*-GaN surface damage.[41] Next, inverted LED structures (*n*-GaN/blue MQWs/*p*-GaN) emitting blue light were regrown on the green LED wafer with the SAG mask pattern using metalorganic chemical vapor deposition (Figure 1a-ii). The most important issue in the regrowth step is minimizing the impact on the underlying green LED structure during the process. The parameters that can affect the green LED structure during regrowth include the regrowth time and the temperature, which could cause degradation of the active region of the green LED structure. To minimize the regrowth influence on the green LED structure, we set the regrowth temperature to 960 °C or less and the regrowth layer thickness to less than 1 μm. After regrowth, the SAG mask patterns were completely removed with a BOE solution to expose the common *p*-GaN region (Figure 1a-iii). Following this, to form the blue pixels and expose the *n*-type GaN layer of the green LEDs, circle etching masks were formed with a larger size (500 μm diameter) than that of the SAG patterns, followed by inductively coupled plasma dry etching. Next, indium tin oxide (ITO) layers were deposited onto the *p*-GaN (green pixel region) and top *n*-GaN (blue pixel region) for current spreading. In this step, we prevented a short circuit

DOI: 10.1021/acsphotonics.8b00876
ACS Photonics XXXX, XXX, XXX−XXX

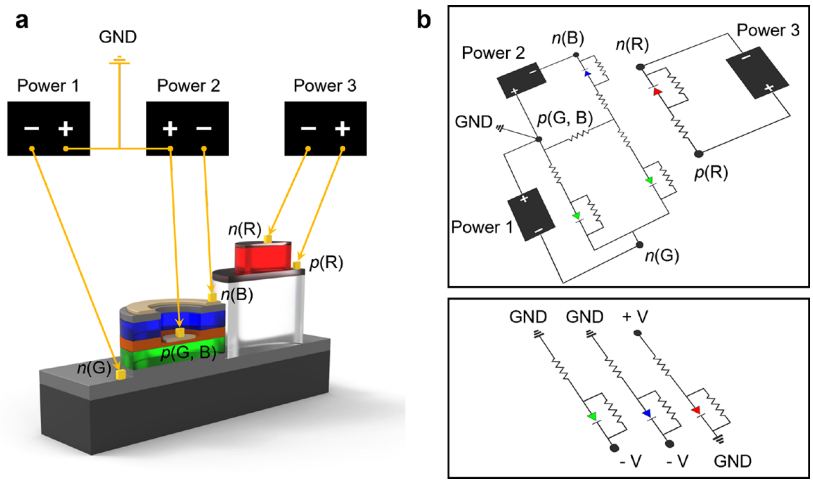


Figure 8. (a) Circuit configuration schematic of the hybrid RGB LEDs and (b) the equivalent circuit diagram of the circuit configuration.

between the common *p*-type and the top *n*-type layers by using ITO patterns with a ∼10 μm gap. Even though the top *n*-GaN layer had a doping concentration as high as $\sim 10^{19}$ cm^{-3}, ITO deposition was nevertheless essential (Supporting Information 4, Figure S3). Finally, the Cr/Au (30/300 nm) layers were evaporated onto the ITO layers and the bottom *n*-GaN layer using an e-beam evaporator for the formation of the *n*- and *p*-type electrodes of the two LEDs.

Integration of AlGaInP-Based LED and GaN-Based LEDs. For realizing the RGB full-color LEDs using the dual LED chip fabricated by the SAG technique, it needs to be combined with an AlGaInP-based red one. In this experiment, we integrated the RGB LEDs using adhesive bonding and substrate removal techniques (Figure 1b). First, before bonding the fabricated dual LEDs and the red LED wafers, the surface treatment of each sample was implemented to improve the surface adhesion of the two samples. For the red LED wafer, the native oxide was removed with diluted HCl solution and then coated with hexamethyldisilazane (HMDS). In the case of the dual LED chip, only the HMDS treatment was performed because the HCl solution could have attacked the metal layer on it. After the surface treatment of the two samples, the adhesive bonding material (SU-8) was coated on the fabricated dual LED chip. Here, the amount of SU-8 needed to be used appropriately depending on the wafer area and the thickness of the bonding layer. Subsequently, the red LED wafer was stacked on the coated dual LED chip so that the two LED epilayers faced each other (Figure 1b-i). To remove any air voids in the SU-8 completely, the laminated sample was placed in a vacuum at room temperature for 1 h before curing (the optimized vacuum time can vary depending on the pattern shape, wafer area, and viscosity of the bonding material). Next, to cure the SU-8, the laminated sample was baked at 200 °C for 2 h in a conduction oven under atmospheric pressure. Afterward, the GaAs substrate was removed and red LED pixels formed, as described in detail in our previous research.[42] Briefly, the GaAs substrate was removed by a NH_4OH-based solution, and the red LED pixels (300 μm diameter circle) were formed using both wet and dry etching processes. Since the cured SU-8 have approximately 90% transmittance, we were able to ensure the location of the blue and green LEDs during the photolithography process of the red LEDs. Figure 1c and d schematically provides top and cross-sectional views of the final device (hybrid RGB LED), respectively. Here, the dimension parameters of the red, green, and blue LEDs are $\pi(150\ \mu m)^2$, $\pi(150\ \mu m)^2$, and $\pi(250\ \mu m)^2 - \pi(150\ \mu m)^2$, respectively. Moreover, the hybrid RGB LEDs have five electrode terminals (one less than individual RGB LED chips), raising the possibility of making the geometric features of the device simpler and smaller.

Circuit Configuration. To achieve full-color emission using the fabricated device, the hybrid RGB LEDs should be independently operated by their respective power sources. We verified the full-color emission of the hybrid RGB LEDs using three power supplies and five probes. In the fabricated device's structure, the blue and green LEDs share a common anode (*p*(G, B)), which is unlike typical LED chip structures, so a special circuit configuration is required to control them independently, as shown in Figure 8a. Here, connecting the *p*(G, B) to GND enables the two LEDs to be individually separated in the circuit, as shown in the equivalent circuit diagram in Figure 8b. As a result, the hybrid RGB LEDs could be independently controlled by their respective power supplies. Figure S4 describes the exceptional emission mode when the monolithic dual LEDs were not individually separated in the circuit (Supporting Information 5, Figure S4).

CONCLUSIONS

We demonstrated the manufacture and a thorough study of hybrid RGB LEDs using SAG and adhesive bonding techniques. These results are significantly meaningful in that all of the inorganic RGB LEDs were integrated on a single wafer, thus, increasing the possibility of their use in compact display applications and reducing costs. The hybrid RGB LEDs could be independently operated with a wide color space (80% of the BT.2020 color space). In the regrowth process, both the epitaxial quality of the regrown epilayer and the MQWs of the underlying epilayer were considered to realize high-quality two-color emission wavelengths. Furthermore, the entire AlGaInP-based thin film was stably transferred without transfer-yield degradation of the red pixels. Overall, we believe that the strategy presented in this study shows great potential for use in various display applications ranging from low-resolution displays to high-resolution ones.

DOI: 10.1021/acsphotonics.8b00876
ACS Photonics XXXX, XXX, XXX−XXX

■ ASSOCIATED CONTENT

Supporting Information

The Supporting Information is available free of charge on the ACS Publications website at DOI: 10.1021/acsphotonics.8b00876.

CIE color coordinates of the hybrid RGB LEDs, EL spectra of the blue LED measured at high injection currents, high-resolution transmission electron microscopy (HRTEM) and fast Fourier transform (FFT) diffraction pattern images of two active regions, photographs of the blue-light emission of the dual LEDs with ITO and without ITO on the top *n*-GaN, and description for the exceptional emission mode of the monolithic dual LEDs (PDF).

■ AUTHOR INFORMATION

Corresponding Author

*E-mail: dslee66@gist.ac.kr. Tel.: 82-62-715-2248. Fax: 82-62-715-2204.

ORCID

Chang-Mo Kang: 0000-0003-0060-2434

Notes

The authors declare no competing financial interest.

■ ACKNOWLEDGMENTS

This study was partly supported by the Ministry of Trade, Industry and Energy (MOTIE) (10067424), the Basic Science Research Program through the National Research Foundation of Korea (NRF) funded by the Ministry of Education under Grant (NRF-2017R1A2B2011858), and Sundiode Inc. The authors wish to thank ETAMAX Inc. for their help with the micro-PL measurements.

■ REFERENCES

(1) Day, J.; Li, J.; Lie, D. Y. C.; Bradford, C.; Lin, J. Y.; Jiang, H. X. III-Nitride Full-Scale High-Resolution Microdisplays. *Appl. Phys. Lett.* **2011**, *99*, 031116.

(2) Tsao, J. Y. Solid-State Lighting: Lamps, Chips and Materials for Tomorrow. *IEEE Circuits Devices Mag.* **2004**, *20*, 28−37.

(3) Pimputkar, S.; Speck, J. S.; DenBaars, S. P.; Nakamura, S. Prospects for LED Lighting. *Nat. Photonics* **2009**, *3*, 180−182.

(4) El-Ghoroury, H. S.; Chuang, C.-L.; Alpaslan, Z. Y. Quantum Photonic Imager (QPI): A Novel Display Technology that Enables more than 3D Applications. *Dig. Tech. Pap. - Soc. Inf. Disp. Int. Symp.* **2015**, *46*, 371−374.

(5) Bower, C. A.; Meitl, M. A.; Raymond, B.; Radauscher, E.; Cok, R.; Bonafede, S.; Gomez, D.; Moore, T.; Prevatte, C.; Fisher, B.; Rotzoll, R.; Melnik, G. A.; Fecioru, A.; Trindade, A. J. Emissive Displays with Transfer-Printed Assemblies of 8 μm × 15 μm Inorganic Light-Emitting Diodes. *Photonics Res.* **2017**, *5*, A23−A29.

(6) Bonar, J. R.; Valentine, G. J.; Gong, Z.; Small, J.; Gorton, S. High-Brightness Low-Power Consumption MicroLED Arrays. *Proc. SPIE* **2016**, *9768*, 97680Y.

(7) Roth, G.-L.; Adelmann, B.; Hellmann, R. Cutting and Drilling of SiC Semiconductor by Fiber Laser. *J. Laser Micro/Nanoeng.* **2015**, *10*, 279−283.

(8) Huang, H.; Wang, S.; Xu, X. Effect of Wire Vibration on the Materials Loss in Sapphire Slicing with the Fixed Diamond Wire. *Mater. Sci. Semicond. Process.* **2017**, *71*, 93−101.

(9) Krames, M. R.; Shchekin, O. B.; Mueller-Mach, R.; Mueller, G. O.; Zhou, L.; Harbers, G.; Craford, M. G. Status and Future of High-Power Light-Emitting Diodes for Solid-State Lighting. *J. Disp. Technol.* **2007**, *3*, 160−175.

(10) Schubert, E. F. Visible-Spectrum LEDs. In *Light-Emitting Diode*, 1st ed; Cambridge University Press: New York, 2003; pp 166−167.

(11) Auf der Maur, M.; Rodrigues, W.; Di Carlo, A.; Pecchia, A.; Penazzi, G. Unraveling the "Green Gap" Problem: The Role of Random Alloy Fluctuations in InGaN/GaN Light Emitting Diodes. *Phys. Rev. Lett.* **2016**, *116*, 027401.

(12) Streubel, K.; Linder, N.; Wirth, R.; Jaeger, A. High Brightness AlGaInP Light-Emitting Diodes. *IEEE J. Sel. Top. Quantum Electron.* **2002**, *8*, 321−332.

(13) Ponce, F. A.; Bour, D. P. Nitride-Based Semiconductors for Blue and Green Light-Emitting Devices. *Nature* **1997**, *386*, 351−359.

(14) Funato, M.; Hayashi, K.; Ueda, M.; Kawakami, Y.; Narukawa, Y.; Mukai, T. Emission Color Tunable Light-Emitting Diodes Composed of InGaN Multifacet Quantum Wells. *Appl. Phys. Lett.* **2008**, *93*, 021126.

(15) Hong, Y. J.; Lee, C.-H; Yoon, A.; Kim, M.; Seong, H.-K.; Chung, H. J.; Sone, C.; Park, Y. J.; Yi, G.-C. Visible-Color-Tunable Light-Emitting Diodes. *Adv. Mater.* **2011**, *23*, 3284−3288.

(16) Tchoe, Y.; Jo, J.; Kim, M.; Heo, J.; Yoo, G.; Sone, C.; Yi, G.-C. Variable-Color Light-Emitting Diodes Using GaN Microdonut Arrays. *Adv. Mater.* **2014**, *26*, 3019−3023.

(17) Lee, M.-L.; Yeh, Y.-H.; Tu, S.-J.; Chen, P. C.; Lai, W.-C.; Sheu, J.-K. White Emission from Non-Planar InGaN/GaN MQW LEDs Grown on GaN Template with Truncated Hexagonal Pyramids. *Opt. Express* **2015**, *23*, A401−A412.

(18) Park, I.-K.; Kim, J.-Y.; Kwon, M.-K.; Cho, C.-Y.; Lim, J.-H.; Park, S.-J. Phosphor-Free White Light-Emitting Diode with Laterally Distributed Multiple Quantum Wells. *Appl. Phys. Lett.* **2008**, *92*, 091110.

(19) El-Ghoroury, H. S.; Yeh, M.; Chen, J. C.; Li, X.; Chuang, C.-L. Growth of Monolithic Full-Color GaN-Based LED with Intermediate Carrier Blocking Layers. *AIP Adv.* **2016**, *6*, 075316.

(20) Yang, G. F.; Zhang, Q.; Wang, J.; Lu, Y. N.; Chen, P.; Wu, Z. L.; Gao, S. M.; Chen, G. Q. InGaN/GaN Multiple Quantum Wells on Selectively Grown GaN Microfacets and the Applications for Phosphor-Free White Light-Emitting Diodes. *Reviews in Physics* **2016**, *1*, 101−119.

(21) Hu, H.-H.; Bibl, A.; Higginson, J. A.; Stephen Law, H.-F. Method of Forming a Micro LED Structure and Array of Micro LED Structures with an Electrically Insulating Layer. U.S. Patent US8,573,469 B2, Nov 5, 2013.

(22) Wu, M.-H.; Fang, Y.-H.; Chao, C.-H. Electric-Programmable Magnetic Module. U.S. Patent US2017/0148650 A1, May 25, 2017.

(23) Kim, T.-I.; Kim, M. J.; Jung, Y. H.; Jang, H.; Dagdeviren, C.; Pao, H. A.; Cho, S. J.; Carlson, A.; Yu, K. J.; Ameen, A.; Chung, H.-J.; Jin, S. H.; Ma, Z.; Rogers, J. A. Thin Film Receiver Materials for Deterministic Assembly by Transfer Printing. *Chem. Mater.* **2014**, *26*, 3502−3507.

(24) Choi, M.; Jang, B.; Lee, W.; Lee, S.; Kim, T. W.; Lee, H.-J.; Kim, J.-H.; Ahn, J.-H. Stretchable Active Matrix Inorganic Light-Emitting Diode Display Enabled by Overlay-Aligned Roll-Transfer Printing. *Adv. Funct. Mater.* **2017**, *27*, 1606005.

(25) Zhang, K.; Peng, D.; Lau, K. M.; Liu, Z. Fully-Integrated Active Matrix Programmable UV and Blue Micro-LED Display System-on-Panel (SoP). *J. Soc. Inf. Disp.* **2017**, *25*, 240−248.

(26) Dupré, L.; Marra, M.; Verney, V.; Aventurier, B.; Henry, F.; Olivier, F.; Tirano, S.; Daami, A.; Templier, F. Processing and Characterization of High Resolution GaN/InGaN LED Arrays at 10 Micron Pitch for Micro Display Applications. *Proc. SPIE* **2017**, *10104*, 1010422.

(27) Lin, H.-Y.; Sher, C.-W.; Hsieh, D.-H.; Chen, X.-Y.; Philp Chen, H.-M.; Chen, T.-M.; Lau, K.-M.; Chen, C.-H.; Lin, C.-C.; Kuo, H.-C. Optical Cross-Talk Reduction in a Quantum-Dot-Based Full-Color Micro-Light-Emitting-Diode Display by a Lithographic-Fabricated Photoresist Mold. *Photonics Res.* **2017**, *5*, 411−416.

(28) Chung, K.; Sui, J.; Demory, B.; Ku, P.-C. Color Mixing from Monolithically Integrated InGaN-Based Light-Emitting Diodes by Local Strain Engineering. *Appl. Phys. Lett.* **2017**, *111*, 041101.

DOI: 10.1021/acsphotonics.8b00876
ACS Photonics XXXX, XXX, XXX−XXX

(29) Kishino, K.; Yanagihara, A.; Ikeda, K.; Yamano, K. Monolithic Integration of Four-Colour InGaN-Based Nanocolumn LEDs. *Electron. Lett.* **2015**, *51*, 852−854.
(30) Kim, T.-I.; Jung, Y. H.; Song, J.; Kim, D.; Li, Y.; Kim, H.-S.; Song, I.-S.; Wierer, J. J.; Pao, H. A.; Huang, Y.; Rogers, J. A. High-Efficiency, Microscale GaN Light-Emitting Diodes and Their Thermal Properties on Unusual Substrates. *Small* **2012**, *8*, 1643−1649.
(31) Chhajed, S.; Xi, Y.; Li, Y.-L.; Gessmann, Th.; Schubert, E. F. Influence of Junction Temperature on Chromaticity and Color-Rendering Properties of Trichromatic White-Light Sources Based on Light-Emitting Diodes. *J. Appl. Phys.* **2005**, *97*, 054506.
(32) Gong, Z.; Jin, S.; Chen, Y.; McKendry, J.; Massoubre, D.; Watson, I. M.; Gu, E.; Dawson, M. D. Size-Dependent Light Output, Spectral Shift, and Self-Heating of 400 nm InGaN Light-Emitting Diodes. *J. Appl. Phys.* **2010**, *107*, 013103.
(33) Liu, Z.; Chong, W. C.; Wong, K. M.; Lau, K. M. GaN-Based LED Micro-Displays for Wearable Applications. *Microelectron. Eng.* **2015**, *148*, 98−103.
(34) Kang, C.-M.; Kong, D.-J.; Shim, J.-P.; Kim, S.; Choi, S.-B.; Lee, J.-Y.; Min, J.-H.; Seo, D.-J.; Choi, S.-Y.; Lee, D.-S. Fabrication of a Vertically-Stacked Passive-Matrix Micro-LED Array Structure for a Dual Color Display. *Opt. Express* **2017**, *25*, 2489−2495.
(35) Parameter Values for Ultra-High Definition Television Systems for Production and International Programme Exchange. *Recommendation ITU-R BT.2020*, 2012.
(36) Chuo, C.-C.; Lee, C.-M.; Chyi, J.-I. Interdiffusion of In and Ga in InGaN/GaN Multiple Quantum Wells. *Appl. Phys. Lett.* **2001**, *78*, 314−316.
(37) Golgir, H. R.; Gao, Y.; Zhou, Y. S.; Fan, L.; Thirugnanam, P.; Keramatnejad, K.; Jiang, L.; Silvain, J.-F.; Lu, Y. F. Low-Temperature Growth of Crystalline Gallium Nitride Films Using Vibrational Excitation of Ammonia Molecules in Laser-Assisted Metalorganic Chemical Vapor Deposition. *Cryst. Growth Des.* **2014**, *14*, 6248−6253.
(38) Geum, D.-M.; Park, M.-S.; Lim, J. Y.; Yang, H.-D.; Song, J. D.; Kim, C. Z.; Yoon, E.; Kim, S.; Choi, W. J. Ultra-High-Throughput Production of III-V/Si Wafer for Electronic and Photonic Applications. *Sci. Rep.* **2016**, *6*, 20610.
(39) Kim, S.; Geum, D.-M.; Park, M.-S.; Kim, H.-S.; Song, J. D.; Choi, W. J. Fabrication of High-Quality GaAs-Based Photodetector Arrays on Si. *Appl. Phys. Lett.* **2017**, *110*, 153505.
(40) Herrnsdorf, J.; McKendry, J. J. D.; Zhang, S.; Xie, E.; Ferreira, R.; Massoubre, D.; Zuhdi, A. M.; Henderson, R. K.; Underwood, I.; Watson, S.; Kelly, A. E.; Gu, E.; Dawson, M. D. Active-Matrix GaN Micro Light-Emitting Diode Display with Unprecedented Brightness. *IEEE Trans. Electron Devices* **2015**, *62*, 1918−1925.
(41) Li, Y.; Yi, X.; Wang, X.; Guo, J.; Wang, L.; Wang, G.; Yang, F.; Zeng, Y.; Li, J. Plasma Induced Damage in GaN-Based Light Emitting Diodes. *Proc. SPIE* **2007**, *6841*, 68410X.
(42) Kang, C.-M.; Kang, S.-J.; Mun, S.-H.; Choi, S.-Y.; Min, J.-H.; Kim, S.; Shim, J.-P.; Lee, D.-S. Monolithic Integration of AlGaInP-Based Red and InGaN-Based Green LEDs via Adhesive Bonding for Multicolor Emission. *Sci. Rep.* **2017**, *7*, 10333.

DOI: 10.1021/acsphotonics.8b00876
ACS Photonics XXXX, XXX, XXX−XXX